AIAA JOURNAL
Vol. 49, No. 2, February 2011

Multifidelity Surrogate Modeling of Experimental and Computational Aerodynamic Data Sets

Yuichi Kuya,* Kenji Takeda,† Xin Zhang,‡ and Alexander I. J. Forrester§
University of Southampton, Southampton, England SO17 1BJ, United Kingdom

DOI: 10.2514/1.J050384

This study presents a multifidelity surrogate modeling approach, combining experimental and computational aerodynamic data sets. A multifidelity cokriging regression surrogate model is used. This study highlights how low-fidelity data from computations contribute to improving surrogate models built with limited high-fidelity data from experiments. Various types of sampling design for low-fidelity data are also examined to study the impact of characteristics of the sampling design on the final surrogate models. Replication, blocking, and randomization techniques originally developed for design of experiments are used to minimize random and systematic errors. Surrogate models representing the performance of an inverted wing with counter-rotating vortex generators in ground effect are constructed, where design variables of the wing ride height and incidence and the response of sectional downforce are examined. A cokriging regression containing 12 experimental and 25 computational data points sampled with a Latin hypercube design shows the best performance here, capturing general characteristics of the target map well.

Nomenclature

A	=	wing planform area
$\boldsymbol{C}$	=	covariance matrix
c	=	wing chord
C_{L_s}	=	sectional downforce coefficient ($2L_s/\rho U_\infty^2 A$)
$\boldsymbol{C_r}$	=	covariance matrix with regression constant
$\boldsymbol{c_r}$	=	covariance vector for prediction with regression constant
$\mathrm{Cor}(\boldsymbol{X}, \boldsymbol{X})$	=	correlation of $\boldsymbol{X}$
$\mathrm{Cov}(\boldsymbol{X}, \boldsymbol{X})$	=	covariance of $\boldsymbol{X}$
L_s	=	sectional downforce
N	=	number of sample data
N_H, N_L	=	number of high- and low-fidelity data
N_v	=	number of verification data
$\boldsymbol{p_d}$, $\boldsymbol{p_L}$, p_i	=	Gaussian process correlation parameter
S_t	=	total uncertainty
U_∞	=	freestream velocity
$\boldsymbol{X}$, X	=	design variable matrix and design variable
$\tilde{\boldsymbol{X}}$	=	augmented design variable matrix
$\boldsymbol{X}^*$	=	vector of unobserved design variable
$\boldsymbol{X_H}$, $\boldsymbol{X_L}$	=	matrix of high- and low-fidelity design variables
x, y, z	=	Cartesian coordinate system; streamwise, vertical, and spanwise directions, respectively
$\boldsymbol{Y}$	=	response value vector
$\hat{\boldsymbol{Y}}$	=	predicted response value vector
$\boldsymbol{Y_H}$, $\boldsymbol{Y_L}$	=	high- and low-fidelity response value vectors
$\boldsymbol{Y_r}$	=	response values in random field
$Z_d(\boldsymbol{X})$, $Z_H(\boldsymbol{X})$, $Z_L(\boldsymbol{X})$	=	Gaussian correlation process
α	=	wing incidence
$\boldsymbol{\theta_d}$, $\boldsymbol{\theta_L}$, θ_i	=	Gaussian process correlation parameter
λ_d	=	regression constant for cokriging regression
$\hat{\mu}_r$	=	optimal mean of normal distribution
ρ	=	air density
ρ_d	=	scaling factor
σ_d^2	=	variance of normal distribution for scaling
$\hat{\sigma}_d^2$	=	optimal variance of normal distribution for scaling
σ_L^2	=	variance of normally distributed low-fidelity data
$\hat{\sigma}_L^2$	=	optimal variance of normally distributed low-fidelity data
$\boldsymbol{\Psi}$	=	correlation matrix
$\boldsymbol{\Psi_d}$	=	correlation matrix for scaling
$\boldsymbol{\Psi_L}$	=	correlation matrix for low-fidelity data

Presented as Paper 2009-2216 at the 5th AIAA Multidisciplinary Design Optimization Specialist Conference, Palm Springs, CA, 4–7 May 2009; received 10 December 2009; revision received 20 September 2010; accepted for publication 23 September 2010.

*Ph.D. Research Student, School of Engineering Sciences. Member AIAA.
†Senior Lecturer, School of Engineering Sciences. Member AIAA.
‡Professor, School of Engineering Sciences. Associate Fellow AIAA.
§Lecturer, School of Engineering Sciences. Member AIAA.

I. Introduction

IN GENERAL, three sorts of aerodynamic testing are performed to develop products in the aeronautical or automobile engineering field: full-scale track testing or flight testing, wind-tunnel testing, and computational simulation [1]. Expensive full-scale testing is often used as a final assessment, with aerodynamic development and analysis relying on wind-tunnel testing to simulate the performance of products. Wind-tunnel testing is, however, relatively expensive to perform in terms of both cost and time. Computational simulations and analysis [i.e., computational fluid dynamics (CFD)] have also been widely applied in the aerodynamic engineering field. However, despite rapid and continuous progress of computational performance and approaches in the past decades, such computations often show discrepancies in results compared with experiments, particularly with low-fidelity computational models. CFD simulations, therefore, are commonly conducted at an initial stage of aerodynamic development, exploring designs that seem good and are subsequently examined by wind-tunnel testing. The same relation can be seen between wind-tunnel testing and full-scale testing; poor candidates are screened out by wind-tunnel testing, and only a few final designs are track or flight tested.

Surrogate modeling is widely used to estimate product performance, particularly in the initial stages of development, due to its ability to significantly reduce the resource requirements for design exploration [2–5]. Although computational data have reduced accuracy, it can generally be obtained with fewer resources, compared with experimental data. Expensive computations may demand a large amount of resources in order to reach a comparable level of accuracy, as experimental testing. To manage such a tradeoff,

the multifidelity surrogate modeling approach has been developed using heterogeneous data sets, such as high- and low-fidelity computational models and experimental and computational simulations. Global trends are captured by low-fidelity models while high-fidelity models are used to correct the global trends, resulting in a surrogate model being closer to the true response function. A great advantage of multifidelity surrogate modeling is that the approach can make the most of the capability of a low-fidelity model being able to obtain many data efficiently and the high precision of a high-fidelity model.

In this study, a multifidelity surrogate model (namely, cokriging regression) is used, combining low-fidelity computational data from CFD simulations and high-fidelity data from wind-tunnel experiments. As mentioned previously, in practice, CFD simulations are performed before wind-tunnel testing. The target of the current study is to use computational data obtained a priori to build an accurate surrogate model with limited high-fidelity wind-tunnel data, which is subsequently available. The impact of the choice of sampling design for the computational data on the final surrogate models is also examined.

A considerable number of studies of multifidelity surrogate modeling have been performed. Haftka [6] and Hutchison et al. [7] performed a multifidelity approximation using some scaling methods. The idea of the methods described is that the ratio or difference between high- and low-fidelity models at one point is calculated as a scaling factor, and the scaling factor is applied to the other low-fidelity data to refine the low-fidelity surrogate model. An autoregressive approach studied by Kennedy and O'Hagan [8] has been exploited in some works, such as Huang et al. [9] and Forrester et al. [10], and is used in the current study. Leary et al. [11] presented a knowledge-based multifidelity approach where low-fidelity data are dealt with as a priori knowledge in the training process of artificial neural networks and kriging interpolation. The knowledge-based approach could achieve a remarkable reduction of computational cost with sufficiently high accuracy, and the kriging interpolation-based approach showed more advantage in terms of ease of construction compared with artificial neural networks. The autoregressive approach presented in Kennedy and O'Hagan [8], however, is more convenient than the knowledge-based approach; the autoregressive approach is applicable to more than two fidelity models, and there is no particular design limitation since the approach uses covariance of a low-fidelity model when inferring a high-fidelity model. Forrester et al. [12] used partially converged simulations as low-fidelity data, which was computed by a high-fidelity model instead of obtaining data from a low-fidelity model. An advantage of this approach is that no separate low-fidelity model is required; thus, the same system can be used to obtain both high- and low-fidelity data.

Although many works (see also [13–16]) have studied multifidelity surrogate modeling, there are fewer studies of multifidelity modeling that combine experimental and computational simulations. An example is Reese et al. [17], where a hierarchical Bayesian integrated modeling approach was used. Experimental data have different characteristics, namely, significant random and systematic errors; therefore, techniques to deal with these errors are demanded. Wind-tunnel experimental data used in this paper are treated as high-fidelity data; hence, replication is employed against random error while blocking and randomization are used in the data sampling process to reduce systematic error. The approach examined here is demonstrated via an example problem of an inverted wing with vortex generators (VGs) in ground effect. In Sec. II, descriptions of the example problem and research methodology used are described. The results and discussion are described in Sec. III followed by conclusions in Sec. IV.

II. Descriptions of Example Problem and Research Methodology

A. Example Problem: Inverted Wing with Vortex Generators in Ground Effect

Multifidelity surrogate modeling is conducted with the wind-tunnel experimental and computational data for an inverted wing with VGs in ground effect, studied in Kuya et al. [18–20]. In open-wheel racing series such as Formula 1 and Indy car racing, inverted wings are used to produce downforce (i.e., negative lift), leading to the enhancement of traction and cornering ability of the cars [1,21]. The performance of aerodynamic devices is altered when operated in close proximity to a solid boundary, known as the ground effect regime, and different flow features are exhibited compared with freestream conditions. Either when a wing is mounted below a particular ride height or has a large wing incidence, a strong adverse pressure gradient is likely to induce flow separation around the trailing edge of the wing suction surface, resulting in considerable energy loss and reduction of the aerodynamic performance. As one of the methods to suppress flow separation in aeronautical applications, VGs can be attached upstream of the separation line [22].

In this study, a configuration of counter-rotating subboundary layer VGs with a device height of 2 mm ($0.009c$) is examined. The VGs are attached on the suction surface of an inverted wing with a constant chord c of 223.4 mm such that the trailing edge of the VGs is fixed at $x/c = 0.537$, as illustrated in Fig. 1. The wing ride height h is altered between $0.090c$ and $0.269c$; meanwhile, the incidence is swept from 1 to 17°.

The experimental data are obtained in the 2.1×1.5 m closed-section wind tunnel at the University of Southampton. The tunnel is of conventional return circuit design and is equipped with a 3.2×1.5 m moving belt rig and a three-component overhead balance system. The moving belt is controlled by slots and a suction system to control the boundary layer, which gives 99.8% of the freestream velocity at 2 mm above the belt. The turbulence intensity of the freestream is approximately 0.3%.

The computational data are obtained by three-dimensional steady Reynolds-averaged Navier–Stokes (RANS) simulations using the Spalart–Allmaras turbulence model [23]. In Kuya et al. [20], the computations used are verified against the experimental results of Kuya et al. [18,19], exhibiting close agreement. The wing used in the experiment has generic endplates at both spanwise ends of the wing, and the force characteristics are affected by the edge vortices induced around the endplates. The computations, however, are performed with a symmetric boundary condition at the spanwise ends of the computational domain; the endplates are not simulated in the computations, corresponding to a sectional simulation around the center portion of the wing where there is no effect of the edge vortices. Accordingly, characteristics of sectional downforce are examined as a response of two design variables: the ride height and incidence. The experimental sectional downforce is calculated by integrating the pressure around the center portion of the wing. Further descriptions regarding the experiments and computations can be found in Kuya et al. [18–20], including uncertainty and verification details.

B. Statistical Techniques in Design of Experiments

In general, wind-tunnel experiments contain random and systematic errors. The field of design of experiments has developed methods minimizing effects of these errors, such as replication, blocking, and randomization.

Random error can be driven down by replication, since random error can be assumed to follow a normal distribution. Systematic

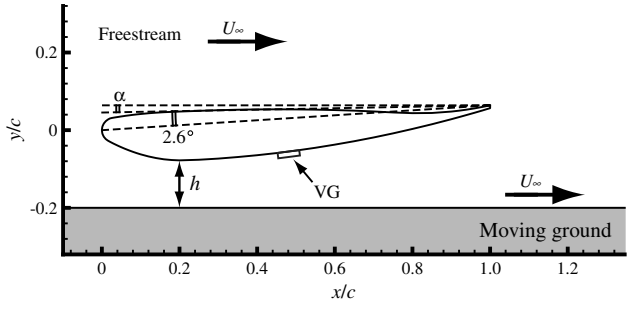

Fig. 1 Schematic of inverted single-element wing and VG.

error is induced by a wide range of factors: for example, in wind-tunnel testing, a shift of air temperature or sensitivity of the force-measurement balance system over the testing period, different wind-tunnel facilities, and different experimental operators who have different skill levels or experience. Systematic error cannot be assumed to be a normal distribution but commonly changes in a particular way in time, leading to a net positive or negative bias. Since it is impossible to find all sources of systematic error and cancel out by replication, blocking and randomization methods are employed here to minimize the effect of systematic error. The procedure grouping a set of experimental units into homogeneous sets (i.e., blocks) is referred to as blocking. The face-centered central composite design (FCD) used for the experimental data here is composed of two blocks: 1) axial and some center points, and 2) corner and some center points. Additionally, the data are randomly taken in each block so that the run order does not correlate with time (i.e., randomization). Although randomization would make samples noisy, the effect of systematic error is driven down by regressing the randomized noisy data with regressing surrogate models [24]. Accordingly, a regressing surrogate model (cokriging regression) is used here. Further descriptions regarding the statistical techniques and design of experiments can be found in DeLoach [24], Fisher [25], and Ryan [26].

C. Sampling Designs

FCD is used for the experimental data while various types of sampling design for the computational data are studied.

Table 1 shows sample data of the wind-tunnel experiments, and Tables 2–5 show samples of the CFD simulations, including the coded design variables of the wing incidence and ride height and their sectional downforce responses. Coded variables, encoded such that the level of all the design variables lies between zero and one, are used in this study. The FCD shown in Table 1 comprises nine sample locations: 12 high-fidelity samples of the wind-tunnel data, including the four time replications at the center point. For the low-fidelity data, four types of sampling designs containing the computational data are examined: 3^2 and 5^2 full factorial design (FFD) and Latin hypercube (LH) with 9 and 25 samples. To ensure a uniform spread of the samples in the design space, the LHs used are optimized by using the Morris–Mitchell criterion [27,28]. As described next, cokriging regression needs at least the same number of low-fidelity samples as that of high-fidelity samples. Although 12 high-fidelity experimental data points are obtained here, the total number of sample locations is the same as the minimum number of low-fidelity computational data points (i.e., nine points) due to the replication at the center point.

D. Cokriging Regression

The following descriptions of cokriging regression are inspired by the works of Forrester et al. [28] and Jones [29].

Cokriging regression is an extension of cokriging interpolation in which the spatial correlation among multiple data sets is calculated. Assume that low- and high-fidelity data sets are given as

Table 1 FCD with 12 experimental samples

Coded design variables		Response
$X_1(=\alpha)$	$X_2(=h/c)$	$Y(=C_{L_s})$
0	0	2.46
0.50	0	1.79
1	0	1.57
0	0.50	1.81
0.50	0.50	1.94
0.50	0.50	1.94
0.50	0.50	1.97
0.50	0.50	1.98
1	0.50	1.33
0	1	1.46
0.50	1	1.80
1	1	1.31

Table 2 3^2 FFD with nine computational samples

Coded design variables		Response
$X_1(=\alpha)$	$X_2(=h/c)$	$Y(=C_{L_s})$
0	0	2.29
0.50	0	1.75
1	0	1.53
0	0.50	1.75
0.50	0.50	1.98
1	0.50	1.78
0	1	1.43
0.50	1	2.57
1	1	1.81

$$\boldsymbol{X} = \begin{pmatrix} \boldsymbol{X_L} \\ \boldsymbol{X_H} \end{pmatrix} = \begin{pmatrix} \boldsymbol{X_L^{(1)}} \\ \vdots \\ \boldsymbol{X_L^{(N_L)}} \\ \boldsymbol{X_H^{(1)}} \\ \vdots \\ \boldsymbol{X_H^{(N_H)}} \end{pmatrix}$$

$$\boldsymbol{Y} = \begin{pmatrix} \boldsymbol{Y_L}(\boldsymbol{X_L}) \\ \boldsymbol{Y_H}(\boldsymbol{X_H}) \end{pmatrix} = \begin{pmatrix} Y_L(\boldsymbol{X_L^{(1)}}) \\ \vdots \\ Y_L(\boldsymbol{X_L^{(N_L)}}) \\ Y_H(\boldsymbol{X_H^{(1)}}) \\ \vdots \\ Y_H(\boldsymbol{X_H^{(N_H)}}) \end{pmatrix}$$

where N_L and N_H are number of the low- and high-fidelity data points, respectively.

To deal with multiple random data sets, the autoregressive model [8] is used, assuming

$$\mathrm{Cov}\left[Y_{rH}(\boldsymbol{X}^{(i)}), Y_{rL}(\boldsymbol{X}) | Y_{rL}(\boldsymbol{X}^{(i)})\right] = 0 \quad \forall\ \boldsymbol{X} \neq \boldsymbol{X}^{(i)} \tag{1}$$

That is, no more can be learned from the low-fidelity data at points where the high-fidelity data are available. A cokriging regression is, however, also constructed for data sets where $\boldsymbol{X_L^{(i)}}$ and $\boldsymbol{X_H^{(i)}}$ are not collocated in this study. In that case, $\boldsymbol{Y_L^{(i)}}$ at $\boldsymbol{X_H^{(i)}}$ is estimated using a low-fidelity kriging interpolation before calculating the likelihood for the high-fidelity data. Assume that a Gaussian process of the high-fidelity data $Z_H(\boldsymbol{X})$ is approximated by a constant scaling factor ρ_d with respect to a Gaussian process of the low-fidelity data $Z_L(\boldsymbol{X})$ and a Gaussian correlation process $Z_d(\boldsymbol{X})$:

$$Z_H(\boldsymbol{X}) = \rho_d Z_L(\boldsymbol{X}) + Z_d(\boldsymbol{X}) \tag{2}$$

Table 3 LH design with nine computational samples

Coded design variables		Response
$X_1(=\alpha)$	$X_2(=h/c)$	$Y(=C_{L_s})$
0.72	0.06	1.69
0.39	0.17	1.86
0.06	0.28	2.17
0.61	0.39	1.94
0.94	0.50	1.80
0.17	0.61	2.22
0.50	0.72	2.28
0.83	0.83	1.94
0.28	0.94	2.28

Table 4 5^2 FFD with 25 computational samples

Coded design variables		Response
$X_1(=\alpha)$	$X_2(=h/c)$	$Y(=C_{L_s})$
0	0	2.29
0.25	0	1.83
0.50	0	1.75
0.75	0	1.62
1	0	1.53
0	0.25	2.00
0.25	0.25	2.59
0.50	0.25	1.91
0.75	0.25	1.82
1	0.25	1.70
0	0.50	1.75
0.25	0.50	2.52
0.50	0.50	1.98
0.75	0.50	1.92
1	0.50	1.78
0	0.75	1.57
0.25	0.75	2.34
0.50	0.75	2.36
0.75	0.75	1.98
1	0.75	1.81
0	1	1.43
0.25	1	2.19
0.50	1	2.57
0.75	1	2.01
1	1	1.81

A covariance matrix for low- and high-fidelity data sets is given as

$$\boldsymbol{C} = \begin{pmatrix} \mathrm{Cov}[\boldsymbol{Y}_{rL}(\boldsymbol{X}_L), \boldsymbol{Y}_{rL}(\boldsymbol{X}_L)] & \mathrm{Cov}[\boldsymbol{Y}_{rL}(\boldsymbol{X}_L), \boldsymbol{Y}_{rH}(\boldsymbol{X}_H)] \\ \mathrm{Cov}[\boldsymbol{Y}_{rH}(\boldsymbol{X}_H), \boldsymbol{Y}_{rL}(\boldsymbol{X}_L)] & \mathrm{Cov}[\boldsymbol{Y}_{rH}(\boldsymbol{X}_H), \boldsymbol{Y}_{rH}(\boldsymbol{X}_H)] \end{pmatrix} \tag{3}$$

In general, covariance is statistically given with a correlation matrix as

$$\mathrm{Cov}\,[\boldsymbol{Y}_r(\boldsymbol{X}), \boldsymbol{Y}_r(\boldsymbol{X})] = \sigma^2 \boldsymbol{\Psi} \tag{4}$$

where

Table 5 LH design with 25 computational samples

Coded design variables		Response
$X_1(=\alpha)$	$X_2(=h/c)$	$Y(=C_{L_s})$
0.50	0.02	1.77
0.14	0.06	2.52
0.42	0.10	1.84
0.06	0.14	2.33
0.18	0.18	2.56
0.62	0.22	1.87
0.74	0.26	1.83
0.86	0.30	1.78
0.38	0.34	2.22
0.58	0.38	1.95
0.22	0.42	2.51
0.34	0.46	2.63
0.94	0.50	1.80
0.54	0.54	1.98
0.30	0.58	2.57
0.90	0.62	1.85
0.02	0.66	1.69
0.82	0.70	1.92
0.26	0.74	2.38
0.70	0.78	2.01
0.46	0.82	2.59
0.98	0.86	1.82
0.10	0.90	1.80
0.78	0.94	1.97
0.66	0.98	2.05

$$\boldsymbol{\Psi} = \begin{pmatrix} \mathrm{Cor}[Y_r(\boldsymbol{X}^{(1)}), Y_r(\boldsymbol{X}^{(1)})] & \cdots & \mathrm{Cor}[Y_r(\boldsymbol{X}^{(1)}), Y_r(\boldsymbol{X}^{(N)})] \\ \vdots & \ddots & \vdots \\ \mathrm{Cor}[Y_r(\boldsymbol{X}^{(N)}), Y_r(\boldsymbol{X}^{(1)})] & \cdots & \mathrm{Cor}[Y_r(\boldsymbol{X}^{(N)}), Y_r(\boldsymbol{X}^{(N)})] \end{pmatrix} \tag{5}$$

$$\mathrm{Cor}[Y_r(\boldsymbol{X}^{(i)}), Y_r(\boldsymbol{X}^{(j)})] = \exp\left(-\sum_{l=1}^{K} \theta_l |X_l^{(i)} - X_l^{(j)}|^{p_l} \right) \quad (i, j = 1, 2, \ldots, N) \tag{6}$$

Accordingly, the covariance matrix of cokriging interpolation is given as

$$\boldsymbol{C} = \begin{pmatrix} \sigma_L^2 \boldsymbol{\Psi}_{\boldsymbol{L}}(\boldsymbol{X}_L, \boldsymbol{X}_L) & \rho_d \sigma_L^2 \boldsymbol{\Psi}_{\boldsymbol{L}}(\boldsymbol{X}_L, \boldsymbol{X}_H) \\ \rho_d \sigma_L^2 \boldsymbol{\Psi}_{\boldsymbol{L}}(\boldsymbol{X}_H, \boldsymbol{X}_L) & \rho_d^2 \sigma_L^2 \boldsymbol{\Psi}_{\boldsymbol{L}}(\boldsymbol{X}_H, \boldsymbol{X}_H) + \sigma_d^2 \boldsymbol{\Psi}_{\boldsymbol{d}}(\boldsymbol{X}_H, \boldsymbol{X}_H) \end{pmatrix} \tag{7}$$

where the Gaussian process correlation parameters $(\boldsymbol{\theta}_{\boldsymbol{L}}, \boldsymbol{\theta}_{\boldsymbol{d}}, \boldsymbol{p}_{\boldsymbol{L}}, \boldsymbol{p}_{\boldsymbol{d}},)$ are estimated for each correlation matrix. A regression constant λ_d is added to the high-fidelity correlation matrix $\boldsymbol{\Psi}_{\boldsymbol{d}}$ to develop cokriging regression so as to drive noise down; the correlation matrix is now $\boldsymbol{\Psi}_{\boldsymbol{d}} + \lambda_d \boldsymbol{I}$, so that $\mathrm{Cor}[Y_r(\boldsymbol{X}_{\boldsymbol{H}}^{(i)}), Y_r(\boldsymbol{X}_{\boldsymbol{H}}^{(j)})] = 1 + \lambda_d$ when $|\boldsymbol{X}_{\boldsymbol{H}}^{(i)} - \boldsymbol{X}_{\boldsymbol{H}}^{(j)}| \to 0$. The covariance matrix of cokriging regression is then given as

$$\boldsymbol{C}_{\boldsymbol{r}} = \begin{pmatrix} \sigma_L^2 \boldsymbol{\Psi}_{\boldsymbol{L}}(\boldsymbol{X}_L, \boldsymbol{X}_L) & \rho_d \sigma_L^2 \boldsymbol{\Psi}_{\boldsymbol{L}}(\boldsymbol{X}_L, \boldsymbol{X}_H) \\ \rho_d \sigma_L^2 \boldsymbol{\Psi}_{\boldsymbol{L}}(\boldsymbol{X}_H, \boldsymbol{X}_L) & \rho_d^2 \sigma_L^2 \boldsymbol{\Psi}_{\boldsymbol{L}}(\boldsymbol{X}_H, \boldsymbol{X}_H) + \sigma_d^2 (\boldsymbol{\Psi}_{\boldsymbol{d}}(\boldsymbol{X}_H, \boldsymbol{X}_H) + \lambda_d \boldsymbol{I}) \end{pmatrix} \tag{8}$$

Vectors $\tilde{\boldsymbol{X}}$ and $\tilde{\boldsymbol{Y}}$ are defined where an unobserved point $\boldsymbol{X}^*$ and its predicted response $\hat{Y}(\boldsymbol{X}^*)$ are added at the $(N_H + 1)$th observation to the original vectors $\boldsymbol{X}$ and $\boldsymbol{Y}$:

$$\tilde{\boldsymbol{X}} = \begin{pmatrix} \boldsymbol{X}_{\boldsymbol{L}} \\ \boldsymbol{X}_{\boldsymbol{H}} \\ \boldsymbol{X}^* \end{pmatrix} = \begin{pmatrix} \boldsymbol{X}_{\boldsymbol{L}}^{(1)} \\ \vdots \\ \boldsymbol{X}_{\boldsymbol{L}}^{(N_L)} \\ \boldsymbol{X}_{\boldsymbol{H}}^{(1)} \\ \vdots \\ \boldsymbol{X}_{\boldsymbol{H}}^{(N_H)} \\ \boldsymbol{X}^* \end{pmatrix}$$

$$\tilde{\boldsymbol{Y}} = \begin{pmatrix} \boldsymbol{Y}_{\boldsymbol{L}}(\boldsymbol{X}_{\boldsymbol{L}}) \\ \boldsymbol{Y}_{\boldsymbol{H}}(\boldsymbol{X}_{\boldsymbol{H}}) \\ Y_H^* \end{pmatrix} = \begin{pmatrix} Y_L(\boldsymbol{X}_{\boldsymbol{L}}^{(1)}) \\ \vdots \\ Y_L(\boldsymbol{X}_{\boldsymbol{L}}^{(N_L)}) \\ Y_H(\boldsymbol{X}_{\boldsymbol{H}}^{(1)}) \\ \vdots \\ Y_H(\boldsymbol{X}_{\boldsymbol{H}}^{(N_H)}) \\ \hat{Y}(\boldsymbol{X}^*) \end{pmatrix}$$

As a result of maximization of the spatial correlation likelihood, a predicted response of cokriging regression at an observed point $\boldsymbol{X}^*$ is given as

$$\hat{Y}(\boldsymbol{X}^*) = \hat{\mu}_r + \boldsymbol{c}_{\boldsymbol{r}}' \boldsymbol{C}_{\boldsymbol{r}}^{-1} (\boldsymbol{Y} - \boldsymbol{1}\hat{\mu}_r) \tag{9}$$

where

$$\hat{\mu}_r = \frac{\boldsymbol{1}' \boldsymbol{C}_{\boldsymbol{r}}^{-1} \boldsymbol{Y}}{\boldsymbol{1}' \boldsymbol{C}_{\boldsymbol{r}}^{-1} \boldsymbol{1}} \tag{10}$$

$$\boldsymbol{c}_{\boldsymbol{r}} = \begin{pmatrix} \rho_d \hat{\sigma}_L^2 \boldsymbol{\psi}_{\boldsymbol{L}}(\boldsymbol{X}_L, \boldsymbol{X}^*) \\ (\rho_d^2 \hat{\sigma}_L^2 + \hat{\sigma}_d^2) \boldsymbol{\psi}_{\boldsymbol{d}}(\boldsymbol{X}_H, \boldsymbol{X}^*) \end{pmatrix} \tag{11}$$

Table 6 Model verification at four verification points regarding response of sectional downforce

	(X_1, X_2)				
	$\begin{pmatrix}0.25\\0.25\end{pmatrix}$	$\begin{pmatrix}0.75\\0.25\end{pmatrix}$	$\begin{pmatrix}0.25\\0.75\end{pmatrix}$	$\begin{pmatrix}0.75\\0.75\end{pmatrix}$	RMSE
True (experiments)	2.42	1.87	2.60	1.75	
Kriging regression ($\text{experiments}_{\text{FCD}}$)	1.75	1.74	1.74	1.74	0.55
Cokriging regression ($\text{experiments}_{\text{FCD}}$ and $\text{computations}_{3^2_{\text{FFD}}}$)	1.99	1.64	1.74	1.61	0.50
Cokriging regression ($\text{experiments}_{\text{FCD}}$ and $\text{computations}_{9\text{LH}}$)	2.03	1.60	1.79	1.55	0.48
Cokriging regression ($\text{experiments}_{\text{FCD}}$ and $\text{computations}_{5^2_{\text{FFD}}}$)	2.37	1.69	1.98	1.55	0.34
Cokriging regression ($\text{experiments}_{\text{FCD}}$ and $\text{computations}_{25\text{LH}}$)	2.51	1.56	2.08	1.51	0.33
Cokriging interpolation ($\text{experiments}_{\text{FCD}}$ and $\text{computations}_{5^2_{\text{FFD}}}$)	2.48	1.69	1.98	1.48	0.35
Cokriging interpolation ($\text{experiments}_{\text{FCD}}$ and $\text{computations}_{25\text{LH}}$)	2.65	1.57	2.09	1.48	0.34

The Gaussian process correlation parameters and ρ_d are numerically estimated by using a genetic algorithm such that the likelihood of the spatial correlation among the samples are maximized, while $\boldsymbol{p_L}$ and $\boldsymbol{p_d}$ are fixed at two; although tuning of $\boldsymbol{p_L}$ and $\boldsymbol{p_d}$ may provide more accurate predictions, some demonstrations have shown good predictions with the fixed value at two.

E. Uncertainty Estimation

An uncertainty estimation of a constructed approximation is necessary to show how much confidence the approximation has at a new point. The estimated total uncertainty of cokriging regression can be calculated as

$$S_t = \sqrt{\rho_d^2\hat{\sigma}_L^2 + \hat{\sigma}_d^2 + \lambda_d - \boldsymbol{c}_r'\boldsymbol{C}_r^{-1}\boldsymbol{c}_r + \frac{(1 - \boldsymbol{1}'\boldsymbol{C}_r^{-1}\boldsymbol{c}_r)^2}{\boldsymbol{1}'\boldsymbol{C}_r^{-1}\boldsymbol{1}}} \tag{12}$$

$$\simeq \sqrt{\rho_d^2\hat{\sigma}_L^2 + \hat{\sigma}_d^2 + \lambda_d - \boldsymbol{c}_r'\boldsymbol{C}_r^{-1}\boldsymbol{c}_r} \tag{13}$$

F. Model Verification

For model verification, four additional sets of data obtained by the experiments are used, and the values are shown at the top column of Table 6 as true. The root-mean-square error (RMSE) is used as a model verification criterion:

$$\text{RMSE} = \sqrt{\frac{\sum_{i=1}^{N_v}(Y^{(i)} - \hat{Y}^{(i)})^2}{N_v}} \tag{14}$$

where N_v is the number of the verification points. A low value of RMSE denotes high accuracy.

III. Results and Discussion

Surrogate models of sectional downforce of an inverted wing with VGs in ground effect are described, where cokriging regressions are built with the high-fidelity data obtained by the wind-tunnel experiment and the low-fidelity data calculated by the RANS computations.

As a reference, a kriging regression shown in Fig. 2 is constructed only with the high-fidelity data. Although it might not be fair to compare the kriging regression with the cokriging regressions that also contain the computational data, the comparison helps to highlight how few the high-fidelity experimental data are used and how much the computational data contribute to improving the surrogate models. As mentioned previously, this study focuses on using the computational data obtained a priori so as to construct better surrogate models with the limited number of experimental data, as in typical design development processes.

Table 6 shows model verifications, listing the true and predicted values at the four verification points and their RMSE. The kriging regression (Fig. 2) shows the poorest accuracy due to the sparsity and location of the high-fidelity data, leading to correlations not being identified; it is known that FCD is not suitable for kriging-based models [30]. The cokriging regressions with the nine computational data points improve accuracy by 9–13% compared with the kriging regression result. Further improvements are obtained by the cokriging regressions with the 25 computational data points, showing approximately 40% improvement in accuracy compared with the kriging regression.

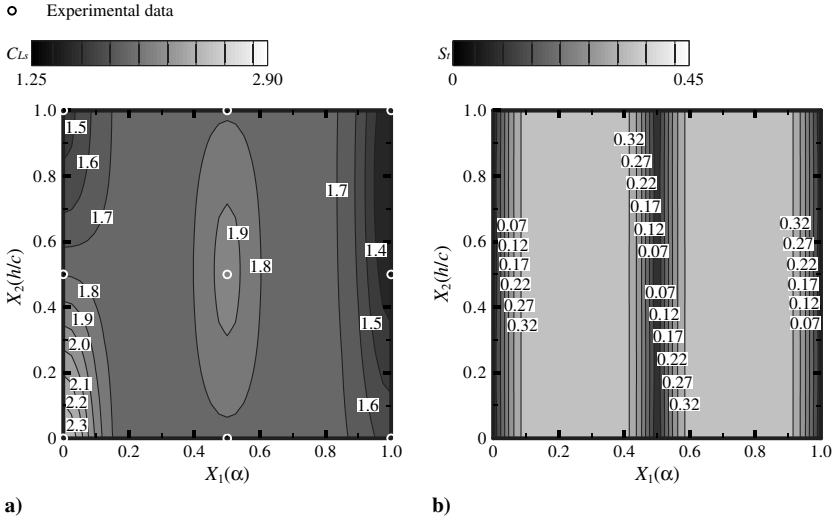

Fig. 2 Kriging regression constructed with 12 FCD experimental samples: a) response approximation and b) total uncertainty.

Figures 3–6 show cokriging regressions built with the experimental data and the computational data, the kriging interpolations for the computational data, and their uncertainty distributions, respectively. The figures apparently highlight effects of the sampling design for the computational data. The 3^2-FFD cokriging regression shown in Fig. 3a predicts high response values around the lower left corner of the design space ($X_1 = 0$ and $X_2 = 0$). Another small local optimum can be seen around $X_1 = 0.50$ and $X_2 = 0.95$. In Fig. 3b, the kriging interpolation built with the computational data indicates poor correlations due to the sampling design used for the low-fidelity data. The nine-LH cokriging regression shown in Fig. 4 yields a similar approximation to that of the 3^2-FFD cokriging regression, while the second optimum shown in the 3^2-FFD cokriging regression is not predicted here. The estimated uncertainty in the nine-LH cokriging regression shown in Fig. 4c is lower than that of the 3^2-FFD cokriging regression shown in Fig. 3c. FFD is not generally suitable for kriging-based models, and space filling designs such as LH are recommended [30]. The cokriging regressions containing the 25 computational samples shown in Figs. 5 and 6 exhibit a wider region of high response values than the 3^2-FFD and nine-LH cokriging regressions. The 5^2-FFD cokriging regression shown in Fig. 5a exhibits an optimum around the lower left corner of the design space ($X_1 = 0$ and $X_2 = 0$) and the other one around slightly higher wing incidence and ride height than the first optimum ($X_1 = 0.25$ and $X_2 = 0.30$). Meanwhile, the first and second optima of the 25-LH cokriging regression are shown around $X_1 = 0.15$ and $X_2 = 0.10$, and $X_1 = 0.30$ and $X_2 = 0.45$, respectively, as shown in Fig. 6a. The 25-LH cokriging regression indicates higher response values around the optima than the 5^2-FFD cokriging regression. The estimated uncertainty of the 5^2-FFD cokriging regression is higher than that of the 25-LH cokriging regression because of the lower likelihood of kriging interpolation for the computational data. The uncertainty of the 25-LH cokriging regression shows an improvement across most of the design space compared with the other surrogate models.

Because the experimental data used contain systematic errors, the regressing surrogate models are employed here to use randomization in order to minimize systematic error statistically. Table 6 also shows the RMSE of cokriging interpolations built with 25 computational samples as references (their approximation maps are not shown here). The cokriging regression shows slightly higher accuracy in terms of RMSE than the cokriging interpolation in the current problem tested here, but it is not possible to say that the improvement

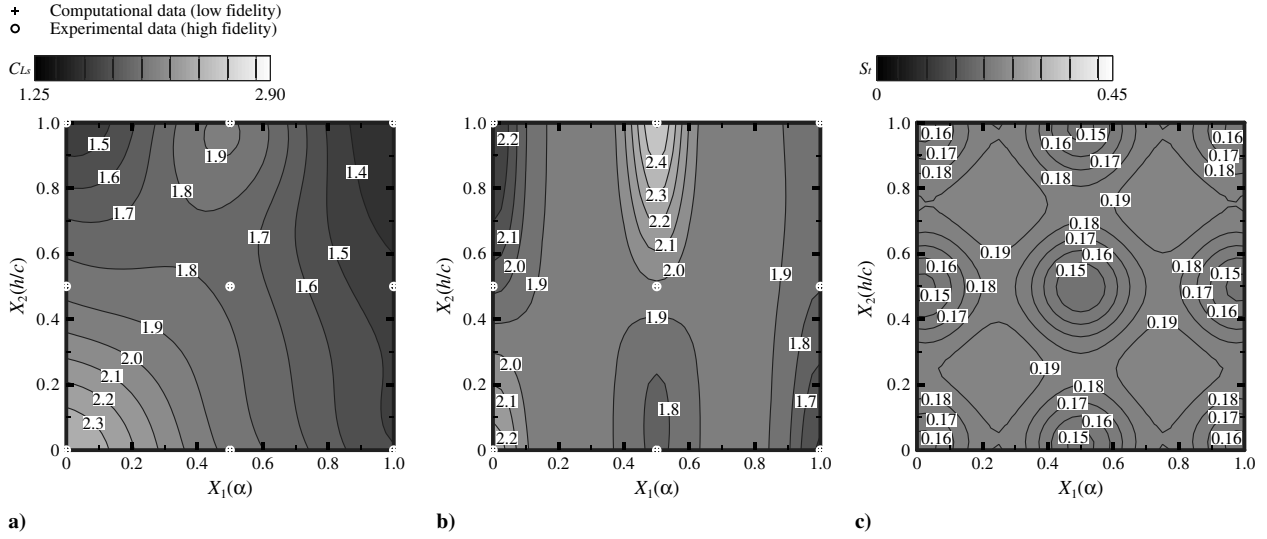

Fig. 3 Cokriging regression constructed with 12 FCD experimental samples and 3^2 FFD computational samples: a) cokriging regression, b) kriging interpolation for low-fidelity data, and c) total uncertainty.

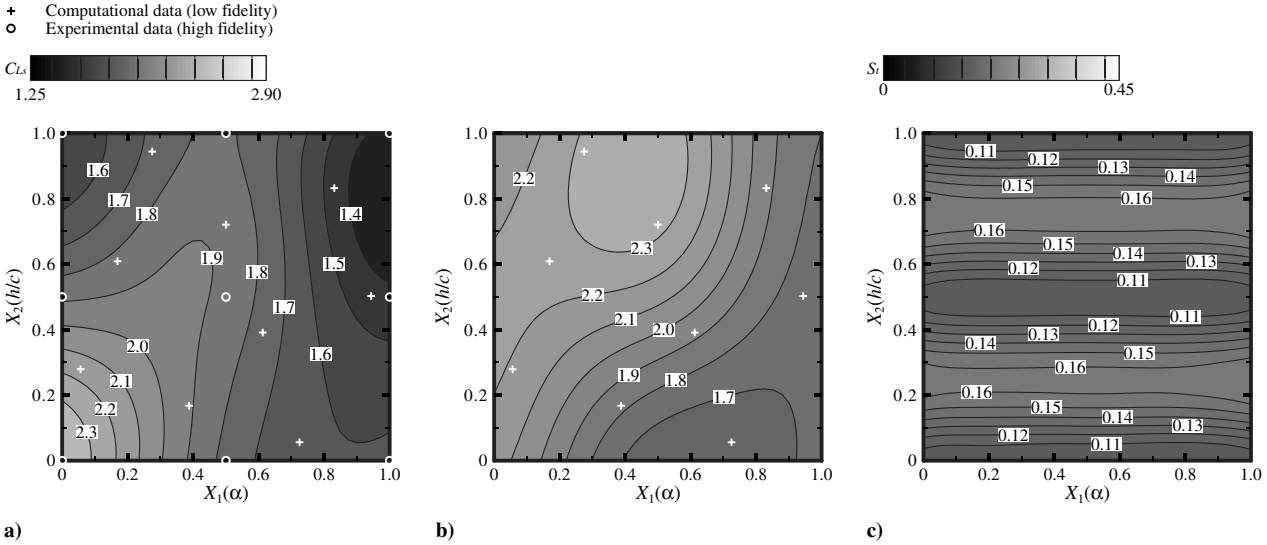

Fig. 4 Cokriging regression constructed with 12 FCD experimental samples and nine LH computational samples: a) cokriging regression, b) kriging interpolation for low-fidelity data, and c) total uncertainty.

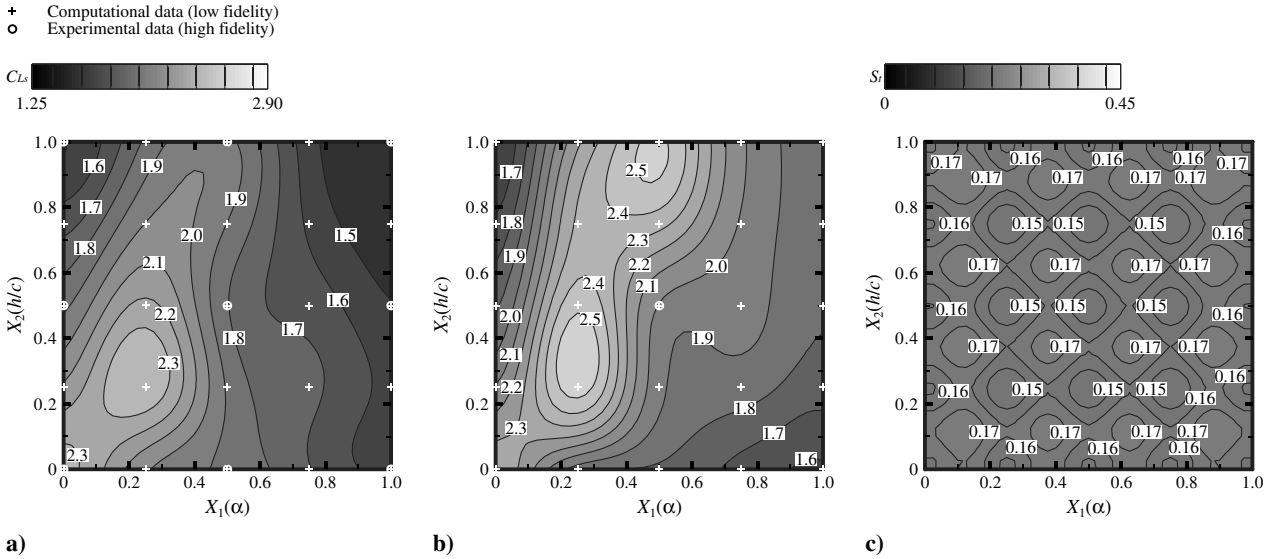

Fig. 5 Cokriging regression constructed with 12 FCD experimental samples and 5^2 FFD computational samples: a) cokriging regression, b) kriging interpolation for low-fidelity data, and c) total uncertainty.

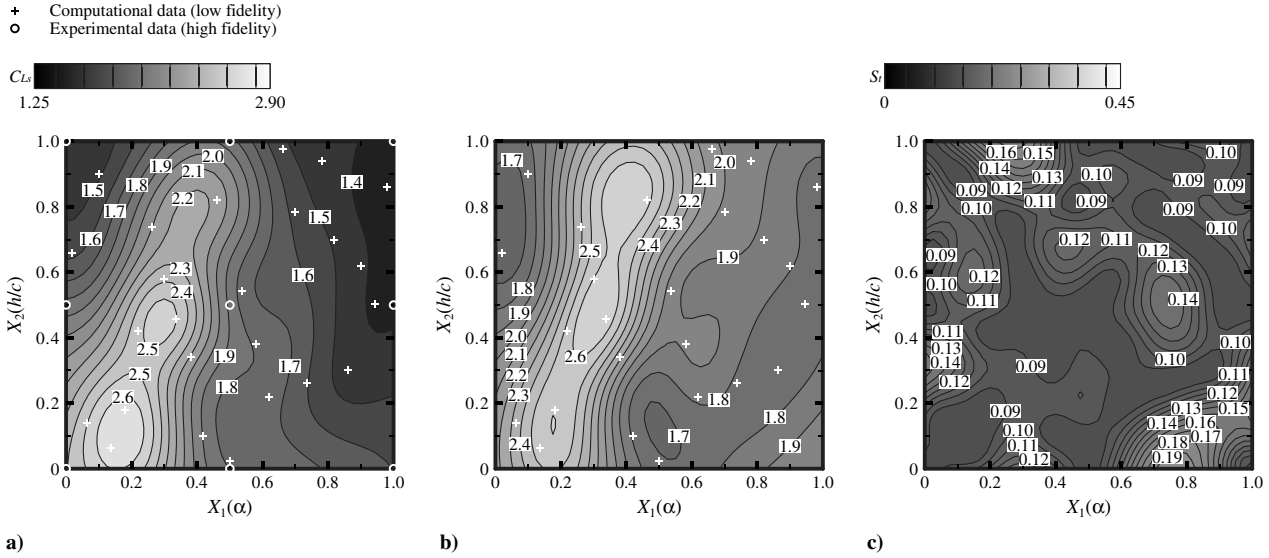

Fig. 6 Cokriging regression constructed with 12 FCD experimental samples and 25 LH computational samples: a) cokriging regression, b) kriging interpolation for low-fidelity data, and c) total uncertainty.

is induced by the suppression of systematic error; the small λ_d leads to a marginal difference between the regression and interpolation models. Cokriging regression, however, has the potential to reduce the effect of systematic error in conjunction with the randomization. Furthermore, blocking is also used with FCD to obtain the high-fidelity experimental data, aiming to reduce systematic error in addition to the randomization; FCD can block systematic error between block boundaries by orthogonal blocking. Although estimating the amount of systematic error reduction via the combination of randomization, regressing models, and blocking is difficult due to the number of sources, those effects have been statistically proven [24,25].

In addition to systematic error, the experimental data used contain random error, and replication is performed at the center point of the FCD used. The replication provides deviation of the samples as 0.02 with 95% confidence, indicating that 95% of new samples should lie within a random error of ± 0.02. Since the replication is performed only at the center point, the samples around the edge may contain random errors, and thus less confidence. The deviation analysis, however, indicates relatively small random error compared with the

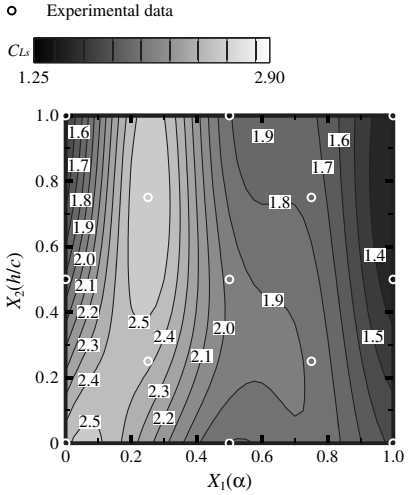

Fig. 7 Target response map constructed with 17 experimental samples built by kriging regression.

Table 7 Optimization of an inverted wing with VGs in ground effect

	First optimum			Second optimum		
	Design variables		Response	Design variables		Response
	α ($\Delta\alpha$, %)	h/c ($\Delta h/c$, %)	C_{L_s} (ΔC_{L_s}, %)	α ($\Delta\alpha$, %)	h/c ($\Delta h/c$, %)	C_{L_s} (ΔC_{L_s}, %)
Target optimum	2.2	0.090	2.54	5.3	0.217	2.60
Kriging regression (FCD)	1.0 (55)	0.090 (0)	2.46 (3)			
Cokriging regression (FCD and 3^2FFD)	1.0 (55)	0.090 (0)	2.34 (8)	8.8 (66)	0.260 (20)	1.91 (27)
Cokriging regression (FCD and 9LH)	1.0 (55)	0.090 (0)	2.40 (6)			
Cokriging regression (FCD and 5^2FFD)	1.0 (55)	0.090 (0)	2.36 (7)	6.1 (15)	0.147 (32)	2.40 (8)
Cokriging regression (FCD and 25LH)	3.7 (68)	0.112 (24)	2.73 (7)	6.1 (15)	0.173 (20)	2.57 (1)

values of sectional downforce themselves in this study and, in general, can provide confidence of experimental samples used for the high-fidelity model, indicating how much the experimental data are scattered due to random error.

Figure 7 shows a target response map constructed by kriging regression with the 17 experimental samples, which are all the experimental data used here: one center point, eight edge points, four axial points outside the design space, and four points used for verification. This target map may not be the true map, but we believe it is our closest representation of the true map. The most accurate approximation built here, in terms of the RMSE, is the cokriging regression constructed with the 12 FCD experimental and 25 LH computational samples, as shown in Fig. 6a, and it is seen that this model does not accurately represent the target map. An important point here, however, is how much the computational data contribute to build the surrogate models with the limited number of the experimental data so as to represent the target map successfully. It is clear that a surrogate model of the kriging regression built with a few experimental data is far from the target map, as shown in Fig. 2a, indicating there is insufficient data to represent the target map. However, in Figs. 2a and 6a, where the same experimental data used are compared, it is apparent how the 25 computational data points contribute to improve the model of the cokriging regression: the best cokriging regression captures the general shape of the target map, including the two comparable optima.

Table 7 summarizes the optimization study of an inverted single-element wing with VGs in ground effect with respect to the maximum sectional downforce. Two optima are presented for the target map, 3^2-FFD, 5^2-FFD, and 25-LH cokriging regressions, while the kriging regression and nine-LH cokriging regressions indicate the optimal configuration only at the lower left corner of the design space, and the second optimum is not captured. The 3^2-FFD cokriging regression predicts the second optimum as $\alpha = 8.8^\circ$ and $h/c = 0.260$, leading to 66 and 20% deviations of the incidence and ride height from the target levels, respectively. The 5^2-FFD cokriging regression shows a smaller deviation of 15% in the incidence, while the ride height is predicted with a larger deviation of 32%. The 25-LH cokriging regression indicates the best prediction here, showing deviations of 15 and 20% in the incidence and ride height, respectively, and a well predicted response with a 1% deviation. The optimal design variables of $\alpha = 6.1^\circ$ and $h/c = 0.173$ are physically reasonable, as described in the experimental and computational studies in Kuya et al. [18–20].

To provide an approximate comparison of the cost effectiveness of the surrogate modeling approach presented, some estimated cost comparisons are given here. Approximate commercial rates for our data are £75[¶] for one wind-tunnel data point and £18[**] for one CFD simulation. When 25 experimental data sets are taken by wind-tunnel testing, this costs £1875. Meanwhile, the best multifidelity surrogate model studied here (i.e., the 25-LH cokriging regression) costs £1350, and extra accuracy can be achieved through the uncertainty-based infill criterion with limited additional cost. The approach suggested, therefore, may save costs if the surrogate model could closely represent the target map.

[¶]Typical closed-section wind-tunnel testing rate.

[**]Fluent remote simulation in November 2009.

These results indicate that the number of samples and type of sampling design for low-fidelity computational data are significant in this multifidelity surrogate modeling approach; therefore, it is prudent to explore optimum updating points added to an initial sampling design. Because low-fidelity data are exploited to represent global trends as a base for high-fidelity approximation in the multifidelity surrogate modeling, an improvement of global accuracy could depend highly on the accuracy of a low-fidelity surrogate model: that is, how close a low-fidelity surrogate model represents general characteristics of the true function. A great advantage of kriging-based models is the capability of providing the uncertainty, and high uncertainty regions are the points where model confidence is less, and thus where update points should be placed. This updating process could help to achieve sufficient accuracy in the low-fidelity surrogate model with a minimum budget, providing a better base of a high-fidelity surrogate model. Further detailed descriptions regarding the uncertainty-based infill criterion can be found in Forrester et al. [28]. Accordingly, we would recommend making a comprehensive plan in advance of considering low-fidelity testing at an initial stage of design developments, constructing reliable low-fidelity surrogate models, and higher-fidelity testing, which will subsequently be performed. In addition, although the multifidelity surrogate modeling of an inverted wing with VGs in ground effect problem has been studied here with some successful results, additional demonstrations might be necessary to assure applicability of the approach. Furthermore, the current study focuses on the advantages of using lower-fidelity data obtained a priori in order to reduce resources of higher-fidelity testing, but further benefits may appear with more than two-level fidelity data, integrating, for example, track-based testing, wind-tunnel testing, and CFD simulations. Finally, it is worth noting that sample points may not be physically realizable due to the inherent lack of flexibility in a physical experimental setup compared with a corresponding computer simulation. For example, a wing incidence is adjusted by a minimum scale, and the sampling design may demand an incidence between the minimum scale. This same problem may occur in the traditional design of experiments. However, cokriging data need not be colocated, and the presence of computational data at the precise desired location (which is not physically realizable) will enhance the prediction in the cokriging model at this point.

The recommended procedure of the multifidelity surrogate modeling studied here can be summarized as follows:

1) Decide sampling design for low-fidelity data. LH is recommended.

2) Obtain the low-fidelity data according to the sampling design.

3) Construct a kriging interpolation with the low-fidelity data.

4) Make sure the low-fidelity surrogate model constructed sufficiently approximates global trend. If not, add updating points using the uncertainty-based infill criterion.

5) Decide sampling design for high-fidelity data. Designs able to use blocking are recommended, such as FCD and nested maximin LH design [31] when the data are obtained by experiments.

6) Obtain the high-fidelity data according to the sampling design using randomization if necessary.

7) Construct a cokriging regression with the low- and high-fidelity data.

8) If updating points are demanded in the high-fidelity model, explore optimum updating points using the uncertainty-based infill criterion.

IV. Conclusions

Multifidelity surrogate modeling of an inverted wing with VGs in ground effect is performed, combining wind-tunnel experimental data and RANS computational data. A multifidelity cokriging regression surrogate model is used. Various types of sampling designs for the low-fidelity data are examined to study how much the low-fidelity data contributes to improving the surrogate model versus only using limited high-fidelity data. A strategy against heterogeneous errors is also shown.

Cokriging regressions with 25 computational data points show higher accuracy than those with nine computational data points, showing lower RMSE. Some of the sampling designs succeed in capturing general characteristics of a target map, with the LH design with 25 computational samples displaying the best performance here. The cokriging regression built with the 12 FCD experimental and 25 LH computational samples indicates a significant improvement in terms of identifying the maximum sectional downforce of an inverted wing with VGs in ground effect compared with the cokriging regressions with the nine computational samples. The best model reduces the difference between the target and prediction from 66 to 15% in the wing incidence, showing a well-predicted response with a 1% deviation. The explored optimal settings are aerodynamically reasonable.

The results indicate a usation of low-fidelity data obtained a priori in practice could reduce the quantity of higher-fidelity data required. The quality of the surrogate model based on the low-fidelity data is, however, a key factor in obtaining an accurate multifidelity surrogate model.

Acknowledgments

Y. Kuya gratefully acknowledges the financial support of the Ministry of Education, Culture, Sports, Science and Technology of Japan and the School of Engineering Sciences at the University of Southampton. The authors would like to thank Mike Tudor-Pole for his assistance throughout the experiments.

References

[1] Zhang, X., Toet, W., and Zerihan, J., "Ground Effect Aerodynamics of Race Cars," *Applied Mechanics Reviews*, Vol. 59, No. 1, 2006, pp. 33–49.
doi:10.1115/1.2110263

[2] Simpson, T. W., Mauery, T. M., Korte, J. J., and Mistree, F., "Kriging Models for Global Approximation in Simulation-Based Multidisciplinary Design Optimization," *AIAA Journal*, Vol. 39, No. 12, 2001, pp. 2233–2241.
doi:10.2514/2.1234

[3] Zink, P. S., Marvis, D. N., Flick, P. M., and Love, M. H., "Impact of Active Aeroelastic Wing Technology on Wing Geometry Using Response Surface Methodology," CEAS/AIAA/ICASE/NASA Langley International Forum on Aeroelasticity and Structural Dynamics, Williamsburg, VA, Georgia Inst. of Technology, Paper , Atlanta, 1999.

[4] Hamstra, J. W., Miller, D. N., Truax, P. P., Anderson, B. A., and Wendt, B. J., "Active Inlet Flow Control Technology Demonstration," *The Aeronautical Journal*, Vol. 104, No. 1040, 2000, pp. 473–479.

[5] Jeyasingham, S., "Vehicle Exterior Aerodynamics Development Using Design of Experiments (DOE)," 2008 World Congress, Society of Automotive Engineers Paper 2008-01-0800, Warrendale, PA, 2008.

[6] Haftka, R. T., "Combining Global and Local Approximations," *AIAA Journal*, Vol. 29, No. 9, 1991, pp. 1523–1525.
doi:10.2514/3.10768

[7] Hutchison, M. G., Unger, E. R., Mason, W. H., Grossman, B., and Haftka, R. T., "Variable-Complexity Aerodynamic Optimization of a High-Speed Civil Transport Wing," *Journal of Aircraft*, Vol. 31, No. 1, 1994, pp. 110–116.
doi:10.2514/3.46462

[8] Kennedy, M. C., and O'Hagan, A., "Predicting the Output from a Complex Computer Code When Fast Approximations Are Available," *Biometrika*, Vol. 87, No. 1, 2000, pp. 1–13.
doi:10.1093/biomet/87.1.1

[9] Huang, D., Allen, T. T., Notz, W. I., and Miller, R. A., "Sequential Kriging Optimization Using Multiple-Fidelity Evaluations," *Structural and Multidisciplinary Optimization*, Vol. 32, No. 5, 2006, pp. 369–382.
doi:10.1007/s00158-005-0587-0

[10] Forrester, A. I. J., Sóbester, A., and Keane, A. J., "Multi-Fidelity Optimization via Surrogate Modelling," *Proceedings of the Royal Society of London, Series A: Mathematical and Physical Sciences*, Vol. 463, No. 2088, 2007, pp. 3251–3269.
doi:10.1098/rspa.2007.1900

[11] Leary, S. J., Bhaskar, A., and Keane, A. J., "A Knowledge-Based Approach To Response Surface Modelling in Multifidelity Optimization," *Journal of Global Optimization*, Vol. 26, No. 3, 2003, pp. 297–319.
doi:10.1023/A:1023283917997

[12] Forrester, A. I. J., Bressloff, N. W., and Keane, A. J., "Optimization Using Surrogate Models and Partially Converged Computational Fluid Dynamics Simulations," *Proceedings of the Royal Society of London, Series A: Mathematical and Physical Sciences*, Vol. 462, No. 2071, 2006, pp. 2177–2204.
doi:10.1098/rspa.2006.1679

[13] Alexandrov, N. M., Nielsen, E. J., Lewis, R. M., and Anderson, W. K., "First-Order Model Management with Variable-Fidelity Physics Applied to Multi-Element Airfoil Optimization," AIAA Paper 2000-4886, 2000.

[14] Rodriguez, J. F., Perez, V. M., Padmanabhan, D., and Renaud, J. E., "Sequential Approximate Optimization Using Variable Fidelity Response Surface Approximations," *Structural and Multidisciplinary Optimization*, Vol. 22, No. 1, 2001, pp. 24–34.
doi:10.1007/s001580100122

[15] Gano, S. E., Renaud, J. E., and Sanders, B., "Hybrid Variable Fidelity Optimization by Using a Kriging-Based Scaling Function," *AIAA Journal*, Vol. 43, No. 11, 2005, pp. 2422–2433.
doi:10.2514/1.12466

[16] Robinson, T. D., Eldred, M. S., Willcox, K. E., and Haimes, R., "Surrogate-Based Optimization Using Multifidelity Models with Variable Parameterization and Corrected Space Mapping," *AIAA Journal*, Vol. 46, No. 11, 2008, pp. 2814–2822.
doi:10.2514/1.36043

[17] Reese, C. S., Wilson, A. G., Hamada, M., Martz, H. F., and Ryan, K. J., "Integrated Analysis of Computer and Physical Experiments," *Technometrics*, Vol. 46, No. 2, 2004, pp. 153–164.
doi:10.1198/004017004000000211

[18] Kuya, Y., Takeda, K., Zhang, X., Beeton, S., and Pandaleon, T., "Flow Separation Control on a Race Car Wing with Vortex Generators in Ground Effect," *Journal of Fluids Engineering*, Vol. 131, No. 12, 2009, Paper 121102.
doi:10.1115/1.4000420

[19] Kuya, Y., Takeda, K., Zhang, X., Beeton, S., and Pandaleon, T., "Flow Physics of a Race Car Wing with Vortex Generators in Ground Effect," *Journal of Fluids Engineering*, Vol. 131, No. 12, 2009, Paper 121103.
doi:10.1115/1.4000423

[20] Kuya, Y., Takeda, K., and Zhang, X., "Computational Investigation of a Race Car Wing with Vortex Generators in Ground Effect," *Journal of Fluids Engineering*, Vol. 132, No. 2, 2010, Paper 021102.
doi:10.1115/1.4000741

[21] Katz, J., "Aerodynamics of Race Cars," *Annual Review of Fluid Mechanics*, Vol. 38, No. 1, 2006, pp. 27–63.
doi:10.1146/annurev.fluid.38.050304.092016

[22] Lin, J. C., "Review of Research on Low-Profile Vortex Generators to Control Boundary-Layer Separation," *Progress in Aerospace Sciences*, Vol. 38, Nos. 4–5, 2002, pp. 389–420.
doi:10.1016/S0376-0421(02)00010-6

[23] Spalart, P. R., and Allmaras, S. R., "A One-Equation Turbulence Model for Aerodynamic Flows," AIAA Paper 1992-0439, 1992.

[24] DeLoach, R., "Improved Quality in Aerospace Testing Through the Modern Design of Experiments," AIAA Paper 2000-0825, 2000.

[25] Fisher, R. A., *The Design of Experiments*, 2nd ed., Oliver and Boyd, Edinburgh, 1947.

[26] Ryan, T. P., *Modern Experimental Design*, Wiley, Hoboken, NJ, 2007.

[27] Morris, M. D., and Mitchell, T. J., "Exploratory Designs for Computational Experiments," *Journal of Statistical Planning and Inference*, Vol. 43, No. 3, 1995, pp. 381–402.
doi:10.1016/0378-3758(94)00035-T

[28] Forrester, A. I. J., Sóbester, A., and Keane, A. J., *Engineering Design via Surrogate Modelling: A Practical Guide*, Wiley, Hoboken, NJ, 2008.

[29] Jones, D. R., "A Taxonomy of Global Optimization Methods Based on Response Surfaces," *Journal of Global Optimization*, Vol. 21, No. 4, 2001, pp. 345–383. doi:10.1023/A:1012771025575

[30] Biles, W. E., Kleijnen, J. P. C., van Beers, W. C. M., and van Nieuwenhuyse, I., "Kriging Metamodeling in Constrained Simulation Optimization: An Explorative Study," *Proceedings of the 2007 Winter Simulation Conference*, IEEE Publ., Piscataway, NJ, 2007, pp. 355–362.

[31] Rennen, G., Husslage, B., Van Dam, E. R., and Den Hertog, D., "Nested Maximin Latin Hypercube Designs," *Structural and Multidisciplinary Optimization*, Vol. 41, No. 3, 2010, pp. 371–395. doi:10.1007/s00158-009-0432-y

T. Zang
Associate Editor